# Slow manifolds and mixed-mode oscillations in the Belousov–Zhabotinskii reaction

Dwight Barkley[a)]
*Center for Studies in Statistical Mechanics and Center for Nonlinear Dynamics, Department of Physics, The University of Texas, Austin, Texas 78712*

(Received 17 June 1988; accepted 20 July 1988)

The mixed-mode oscillations observed at high flow rates in the Belousov–Zhabotinskii (BZ) reaction are considered and comparison is made between these oscillations and the dynamics of three different mathematical models based on slow manifolds. It is shown that the model proposed by Rössler for the generation of complex behavior in nonequilibrium chemical reactions is in conflict with the behavior of the BZ reaction. It is also shown that a slow-manifold model based on the hysteresis-Hopf normal form fails to accurately reproduce the oscillations found at high flow rates in the BZ system. A model of the type first proposed by Boissonade is presented; the model consists of the coupling of two simple systems. It is shown that this model naturally generates mixed-mode oscillations like those observed in the BZ reaction.

## I. INTRODUCTION

Nonequilibrium chemical systems are often governed by many component reactions whose time scales range over several orders of magnitude. These differing time scales result in slow manifolds in the state spaces of many chemical systems. This is illustrated in Fig. 1 where we show the slow manifold and steady state for a hypothetical reaction evolving three chemical species. The state-space coordinates correspond to the concentration of the species in a homogeneous reactor. While on the slow manifold, the system evolves by some relatively slow process. If, however, the system passes over a pleat, or is otherwise in a state that does not lie on the slow manifold, then a fast process takes over, causing concentrations to quickly adjust and bring the system back to the surface shown.

Much of the dynamics exhibited by chemical reactions has been modeled[1–9] using *S*-shaped or pleated slow manifolds like that illustrated in Fig. 1. These slow-manifold models provide simple geometrical pictures of the variety of dynamics found in experiments and in simulations of larger, chemically based models.

The slow-manifold models used to describe the chemical reactions fall mainly into one of two types, which we shall refer to as the Rössler and Boissonade types, after the authors who first (and almost simultaneously) introduced them.[1,2] While models of both types are based on *S*-shaped slow manifolds, there are differences between the two which are of fundamental importance for explaining the dynamics of chemical reactions. Apart from a brief discussion by De Kepper and Boissonade,[10] these important distinctions have not been stressed.

The purpose of this paper is to review and contrast different slow-manifold models. In particular, we shall show that, initial appearances to the contrary, Fig. 1 provides an incorrect picture for the mixed-mode oscillations of the Belousov–Zhabotinskii (BZ) reaction. While our study focuses on the BZ reaction, we believe that many of our findings hold for other chemical reactions as well. (For a review of slow-manifold models different from those considered here, see Rinzel.[11])

Because we incorporate into our discussion many models as well as experimental results, a few words are in order concerning the organization of the paper. Our approach shall be to compare the dynamics of experiments and simulations of the BZ reaction with the dynamics of three mathematical models based on slow manifolds: the Rössler model, the hysteresis-Hopf normal form, and a model of the Boissonade type.

We begin by considering the complex dynamics found at high flow rates in the BZ reaction; this includes results both from experiments and from simulations of an Oregonator model[12] of the reaction. We then describe the Rössler slow-manifold picture and compare and contrast the dynamics of Rössler models with that of the BZ reaction. We look briefly at a slow-manifold model based on the hysteresis-Hopf normal form. This model is similar to those of the Rössler type, but is sufficiently different to warrant a separate treatment.

We then present a model of our own design, which we call model A, based on the coupling of two simpler models. Using this model, we discuss the Boissonade slow-manifold picture and show that it naturally generates most features of

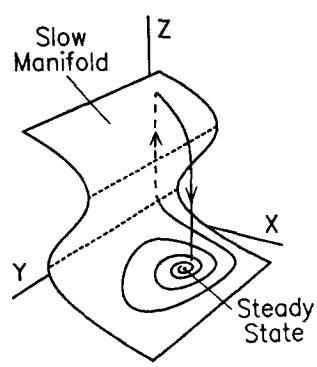


FIG. 1. Illustration of a slow manifold in the state space of a hypothetical chemical reaction. The coordinates represent the concentrations of chemical species in a homogeneous reaction. The steady state is stable transverse to the slow manifold and unstable along it. The trajectory illustrates the evolution typical of such a system.

[a)] Present address: Applied Mathematics, California Institute of Technology, Pasadena, California 91125.

 0021-9606/88/215547-13$02.10  

the BZ dynamics. Finally, in the Appendix we present a gallery of interesting states found in model A.

## II. MIXED-MODE OSCILLATIONS IN THE BZ REACTION

Our ultimate goal is formulating the proper slow-manifold picture for the mixed-mode oscillations found at high flow rates in the BZ reaction. Therefore, we begin with a discussion of these oscillations in experiments and simulations.

### A. Experiment

Shown in Fig. 2 are results obtained by Hudson *et al.*[13] in experiments on the BZ reaction in a well-stirred flow reactor. We shall refer to the multipeaked states shown as mixed-mode oscillations, for they are composed of mixtures of two distinct modes of oscillation: small-amplitude nearly harmonic oscillations and large-amplitude relaxation oscillations.

Figure 3 (from Hudson *et al.*[14]) provides an excellent illustration of the variety of oscillations that can be observed as a control parameter is varied. Representative time series are shown at several values of the control parameter (flow rate). The other constraints (feed concentrations, temperature, etc.) are the same as those of Fig. 2.

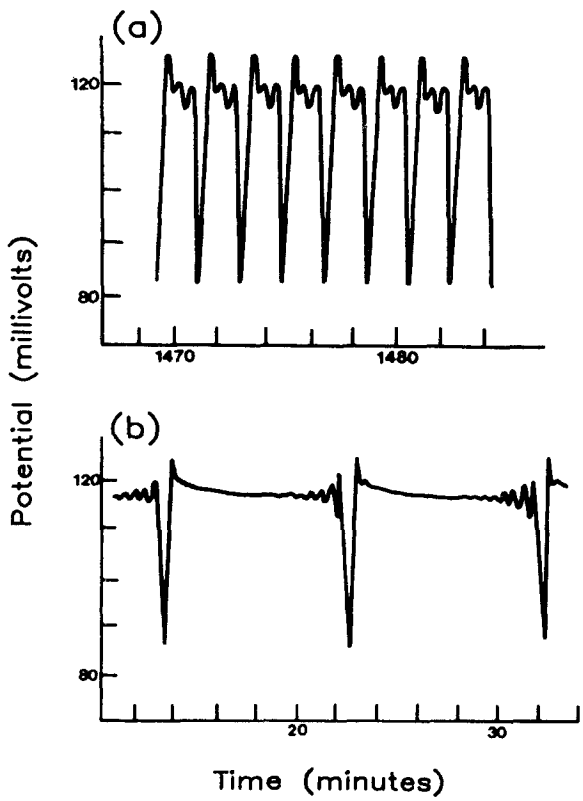


FIG. 2. Representative mixed-mode oscillations from experiments on the BZ reaction in a CSTR. Shown is the output of a bromide-ion electrode as a function of time at two different flow rates. The flow rate in (a) is 4.34 ml/min and in (b) is 5.37 ml/min (see Fig. 3). Reproduced with permission from Hudson, Hart, and Marinko (Ref. 13).

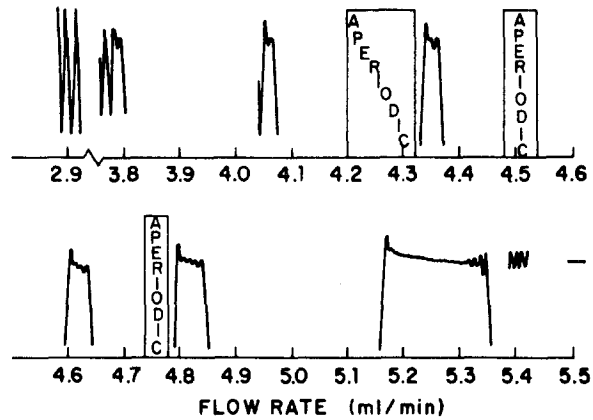


FIG. 3. Summary of states as a function of flow rate from experiments on the BZ reaction in a CSTR. Representative time series are shown at several flow rates. The experimental conditions are the same as in Fig. 2. Reproduced with permission from Hudson, Marinko, and Dove (Ref. 14).

It is evident from Fig. 3 that as flow rate is increased there is an increase in ratio of small to large oscillations in the mixed-mode states. At high flow rates (5.4 ml/min) there is a transition from mixed-mode to small oscillations, and above this (5.5 ml/min), there is a transition to steady state.

The state shown in Fig. 2(b) is that found just before the transition to small oscillations. For reasons which will be clear, we shall refer to this as a spiral state or spiral attractor. It is characterized by long periods of quiescence, followed by growing small oscillations and then a relaxation oscillation. Decaying small oscillations are sometimes observed to precede the period of quiescence. The spiral attractor provides important insight into the proper slow-manifold picture of the BZ reaction. The dynamics associated with this state will be the main focus of our analysis.

### B. The SNB model

While the experimental observations are of principal importance, they provide only limited information. Generally in experiment, the concentration of a single chemical species is measured as a function of time. Furthermore, the study of transients, which gives important information for the evaluation of slow-manifold models, is experimentally difficult.

To overcome these difficulties, we turn to a model of the BZ reaction which is of chemical origin, and which provides simulation of the behavior of interest. Note that our use of this *chemical model* is different from our use in later sections of models based on slow manifolds: here we simulate, as accurately as possible, the dynamics of the chemistry; in subsequent sections we use simple geometrical models to obtain insight into this dynamics.

The model we employ is due to Showalter, Noyes, and Bar-Eli (SNB)[12]; it is a modification of the original Oregonator proposed by Field and Noyes.[15] (SNB originally introduced the model, in part, to account for the variety of oscillations observed by Hudson *et al.*) The model consists of the following six reaction steps:

$$A + Y \underset{k_{-1}}{\overset{k_1}{\rightleftarrows}} X + P, \quad X + Y \underset{k_{-2}}{\overset{k_2}{\rightleftarrows}} 2P,$$

$$A + X \underset{k_{-3}}{\overset{k_3}{\rightleftarrows}} 2W, \quad C + W \underset{k_{-4}}{\overset{k_4}{\rightleftarrows}} X + Z,$$

$$2X \underset{k_{-5}}{\overset{k_5}{\rightleftarrows}} A + P, \quad Z \overset{k_6}{\rightarrow} gY + C,$$

where $A \equiv BrO_3^-$, $Y \equiv Br^-$, $X \equiv HBrO_2$, $P \equiv HOBr$, $W \equiv BrO_2\cdot$, $Z \equiv Ce^{4+}$, $C \equiv Ce^{3+}$. (Note that we shall use these same capital letters to denote the concentrations of the corresponding chemical species; the meaning will be clear from the context.) This kinetic scheme gives rise in the usual way to a system of coupled ordinary differential equations for the concentrations of the chemical species in a well-stirred flow reactor.

We use the values originally given by SNB for the rate constants of the first five reactions:

$$k_1 = 0.084, \quad k_{-1} = 1.0\times10^4,$$
$$k_2 = 4.0\times10^8, \quad k_{-2} = 5.0\times10^{-5},$$
$$k_3 = 2.0\times10^3, \quad k_{-3} = 2.0\times10^7,$$
$$k_4 = 1.3\times10^5, \quad k_{-4} = 2.4\times10^7,$$
$$k_5 = 4.0\times10^7, \quad k_{-5} = 4.0\times10^{-11}.$$

These constants are in $M^{-1}\,s^{-1}$ and assume $[H^+] = 0.2$ M. Unless stated otherwise, the following values are assigned to the remaining model parameters:

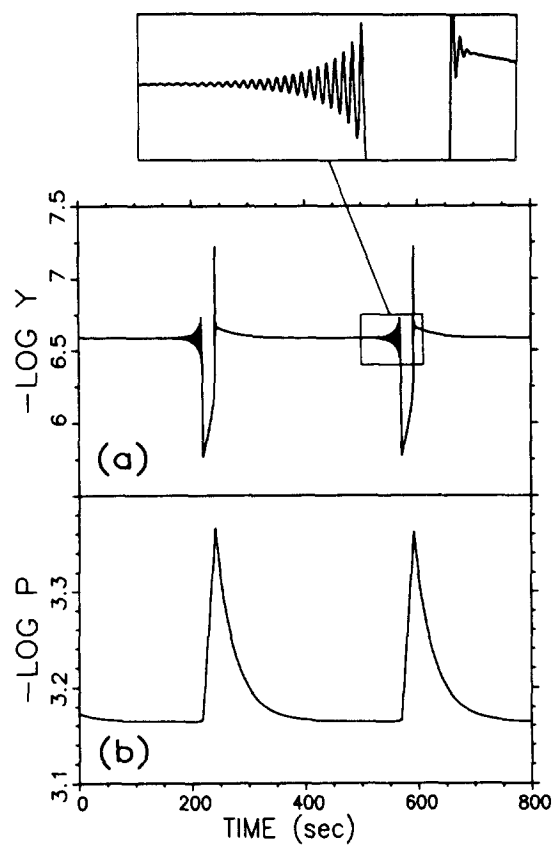


FIG. 4. Mixed-mode oscillations obtained from the SNB model. This state is similar to that seen in experiment [Fig. 2(b)]. Enlarged are the small oscillations which precede and follow the relaxation oscillations.

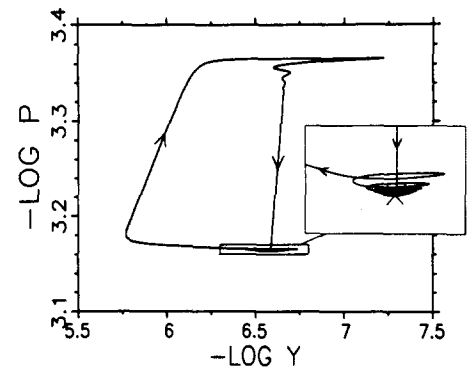


FIG. 5. Phase portrait for the mixed-mode state shown in Fig. 4. The enlargement shows the spiral nature of the attractor associated with these oscillations. The × marks a saddle-focus fixed point.

$$k_0 = 2.1\times10^{-2}\,s^{-1},\ k_6 = 2.9\,s^{-1},\ g = 0.42,$$
$$A_0 = 0.14\ M,\ C_0 = 2.7\times10^{-4}\ M,\ Y_0 = 1.0\times10^{-7}\ M, \quad (1)$$

where $k_0$ = flow rate/reactor volume, and $A_0$, $C_0$, and $Y_0$ denote the feed concentration of $BrO_3^-$, $Ce^{3+}$, and $Br^-$, respectively. All other feed concentrations are zero. All results for the SNB model, and for model A presented in Sec. V, have been obtained by numerical integration using the Gear method (IMSL subroutine DGEAR[16] modified for relative-error checking), with a one-step error tolerance of $10^{-10}$.

In Figs. 4 and 5 we show a numerically generated mixed-mode state similar to that seen in experiment [Fig. 2(b)]. We show time series for the concentrations of Y and P in Fig. 4 and a phase portrait of the associated spiral in Fig. 5. To allow for comparison with experiment,[17] we have plotted $-\log Y$ as a function of time in Fig. 4(a). We have also plotted $-\log P$ on the ordinate of Fig. 5 [and of the ordinate of Fig. 4(b)], so that the spiral attractor is oriented with the growing small oscillations at the bottom of the phase portrait. We shall follow this convention when presenting other spiral states (e.g., Fig. 1).

The spiral lies extremely close to a saddle-focus fixed point (three negative real eigenvalues and a complex conjugate pair of eigenvalues with positive real part). This fixed point is shown in the enlargement of the phase portrait. The attractor associated with the oscillations in Fig. 4 (and presumably Fig. 2) is thus very nearly a homoclinic orbit. However, the oscillations are not of infinite period, and therefore the spiral is, in fact, not homoclinic. Simulations of the spiral are very susceptible to numerical "noise," however, and it is difficult to ascertain whether the spiral is exactly a periodic state, and if so, its period.

While the BZ spiral resembles that analyzed by Šilnikov,[18] it does not meet the Šilnikov condition for chaos (see Guckenheimer and Holmes,[19] and Argoul *et al.*[9]). That is, in the SNB model (for the parameters we consider), the time scale by which trajectories approach the saddle focus is slower than the time scale by which they leave. This is contrary to the hypotheses of the Šilnikov theorem guaranteeing complex dynamics near homoclinic orbits. As will be seen, this slow approach to the saddle focus in the BZ system is of fundamental importance.

The expanded portion of the time series emphasizes the small oscillations. The period of these oscillations is smaller than in experiment. This discrepancy, a characteristic of the SNB model, will not be of importance here. The enlargement also shows the decaying small oscillations immediately following the relaxation oscillation. These decaying oscillations are seen at the top of the phase portrait. Similar small oscillations are seen in the experimental time series [Fig. 3 and just after the second and third relaxation oscillation in Fig. 2(b)]. In the simulation, the first of these decaying oscillations is seen as a large (low bromide-ion) spike in the time series. This large spike does not appear in the experimental time series (see Ref. 17).

As the flow rate in the simulation is decreased below that of Fig. 4, the ratio of small to large oscillations decrease until only large oscillations are found. As the flow rate is increased slightly above that for the spiral state, the system makes a transition to small oscillations and then to steady state via a Hopf bifurcation. Both of these facts are in accord with experiment (Fig. 3). Therefore, we take the model dynamics to be a good representation of that observed in experiment.

We note, however, that the SNB model does not reproduce (for the parameters we consider) the chaos reported experimentally (i.e., the chaotic regions in Fig. 3). This absence of chaos in simulations is well documented,[20–22] and is consistent with the Šilnikov condition discussed above. However, Lindberg[23] does report chaos in the SNB model similar to that seen in experiments at *low flow rates*. Chaos has also been observed in the SNB model between small and mixed-mode oscillations.[24] While the question of chaos in chemical reactions is important, it is outside the focus of this paper and we shall only touch upon it as needed.

The behavior illustrated in Figs. 2–5, specifically the spiral attractor and the sequence of transitions, mixed-mode oscillations → small oscillations → steady state, has been observed at high flow rates in both experiments and simulations for a variety of conditions in addition to those shown.[6,24–28] Thus, while other behavior might be possible, the spiral should be thought of as characteristic of the high flow-rate dynamics of the BZ reaction and not specific to the parameters selected here. The remainder of the paper is devoted to the interpretation this behavior in terms of simple slow-manifold models.

## III. THE RÖSSLER PICTURE

We now examine the slow-manifold picture due to Rössler.[1] This is the picture illustrated in the introduction (Fig. 1). We shall show that while this picture would seem to explain the mixed-mode oscillations in the BZ reaction, it in fact, does not.

### A. The Gaspard–Nicolis equations

Several different reaction schemes and mathematical models based on the original ideas of Rössler have been put forth. Gaspard and Nicolis[29] have introduced a system of equations, deriving from mass-action kinetics, which is particularly well suited for illustrating the Rössler model.

The Gaspard–Nicolis equations are

$$\dot{x} = x(dx - fy - z + g), \tag{2a}$$

$$\dot{y} = y(x + sz - l), \tag{2b}$$

$$\dot{z} = \frac{1}{\epsilon}(x - az^3 + bz^2 - cz). \tag{2c}$$

We shall often refer to Eqs. (2) as the Rössler model. Most of the results which we report for this model have been obtained with parameter values investigated by Gaspard and Nicolis, namely

$$a = 0.5,\ b = 3.0,\ c = 5.0,$$
$$f = 0.5,\ g = 0.6,\ l = 1.3,$$
$$s = 0.3,\ \epsilon = 0.01, \tag{3}$$

with $d$ taken as an adjustable control parameter.

The first requirement of models of the Rössler type is a pleated slow manifold. Together, the cubic nature of the $\dot{z}$ equation and the smallness of the parameter $\epsilon$ provide such a slow manifold in Eqs. (2). The quantity $|\dot{z}|$ is large in comparison with $|\dot{x}|$ and $|\dot{y}|$, except when the right-hand side of Eq. (2c) is near zero. Thus setting $\dot{z} = 0$, we obtain the following expression for the slow manifold:

$$x = az^3 - bz^2 + cz. \tag{4}$$

This is the surface shown in Fig. 1. Note that only the upper and lower sheets are attracting; small perturbations will drive the system off the middle sheet.

In addition to the pleated manifold, the Rössler picture requires a saddle-focus fixed point on one of the stable sheets of the manifold (the lower sheet in Fig. 1). The fixed point is unstable with oscillatory behavior along the slow manifold. Due to the attraction to the manifold, the fixed point is stable in a transverse direction.

The system evolves in time as follows: orbits starting near the saddle focus spiral away on the slow manifold until they reach the lower pleat. They then jump to the upper sheet where they again move slowly. The pleats are arranged in such a way that trajectories are reinjected back onto the lower sheet in the vicinity of the fixed point, and the process repeats. Depending on the system parameters, the resulting behavior may be periodic or chaotic (see Fig. 6 discussed below).

### B. Similarities between the Rössler and BZ dynamics

Early on, Schmitz, Graziani, and Hudson[3] realized that a slow-manifold model, like that proposed by Rössler, could be used to explain the multipeaked oscillations observed in the BZ reaction (see also Tyson[4] and Maselko[6]). The nearly harmonic oscillations are attributed to spiraling from the saddle focus, and relaxation oscillations with jumps between the sheets of the slow manifold.

Schmitz *et al.* further noted that the slow manifold could be used to explain the variety of states observed in experiments (e.g., Fig. 3). Their interpretation of experimental results is illustrated in Fig. 6 with states obtained from Eqs. (2). We shall describe the correspondence between the states shown in Fig. 6 and experimental results shown in Fig. 3 in order of decreasing flow rate. [Fig. 6(a)

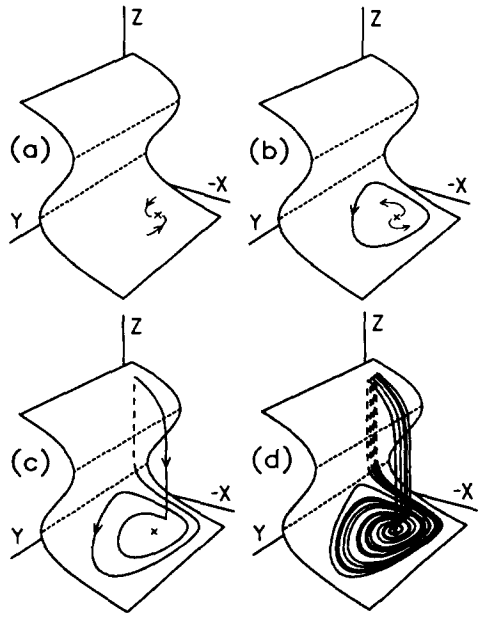


FIG. 6. Sequence of states for the Rössler slow-manifold picture. States were obtained from Eqs. (2) with (a) $d = 0.26$: stable fixed point; (b) $d = 0.35$: unstable fixed point and small-amplitude limit cycle; (d) $d = 0.49$: periodic mixed-mode state; and (d) $d = 0.51$: chaotic mixed-mode state. The coordinate axes shown are not centered on the origin, and the $x$-axis point in the direction of decreasing values.

corresponds to high flow rates, and Fig. 6(d) to low flow rates.]

At high flow rates, the BZ reaction exhibits a stable steady state, and as the flow rate is decreased, this steady state gives way to small oscillations. In the Rössler picture, this simply corresponds to a stable steady state on the slow manifold [Fig. 6(a)] becoming unstable to nearly harmonic oscillations [Fig. 6(b)] via a Hopf bifurcation.

As the flow rate is lowered in experiments, the amplitude of the small oscillations grows until there is a transition to mixed-mode oscillations. In the Rössler picture, this corresponds to the amplitude of the limit cycle growing as a function of a control parameter (as it does after a Hopf bifurcation), until the limit cycle reaches the pleat and "falls off the edge" [Fig. 6(c)].

The Rössler picture can also account for the decrease in the ratio of small to large oscillations seen in experiment. Corresponding to the growth in amplitude of the limit cycle as a function of parameter, there is a growth in the rate at which trajectories leave the vicinity of the fixed point. Specifically, the real part of the complex pair of eigenvalues associated with the Hopf bifurcation grows, while the imaginary parts of these eigenvalues remain approximately constant. Thus, one expects fewer small orbits on the lower sheet of the slow manifold per reinjection.

Finally, as in experiment, there are parameter intervals in the Rössler model for which chaos is observed [Fig. 6(d)]. (Rössler, in fact, originally introduced slow-manifold models to generate chaotic dynamics.)

### C. Differences between the Rössler and BZ dynamics

It would appear that the original Rössler mechanism provides a very comprehensive picture of the mixed-mode dynamics in the BZ reaction; however, this is not so. While much of the interpretation of Schmitz *et al.* is correct, the orientation of the slow manifold in the BZ system is not as in the Rössler picture. In this section we note three major discrepancies between the Rössler model and the BZ system; in Sec. V we show how these problems are overcome with a different slow-manifold model.

(i) The most fundamental difference between the BZ and Rössler dynamics concerns the time dependence of the *reinjection variable*: the variable corresponding most closely to the direction along which the system returns to the steady state. For the BZ system (specifically the SNB model), this variable is the concentration $P$ (see Fig. 5). For the Rössler model [Eqs. (2)], $z$ is the reinjection variable. In Fig. 7 we show a portion of a time series for $z$ with $d = 0.51$.

The behavior of the SNB model [Fig. 4(b)] is entirely different from that of the Rössler picture (Fig. 7). In the SNB model, the approach to the saddle focus is slow. That is, the decay is governed by the slowest time scale associated with the fixed point. (The eigenvalue closest to zero is approximately $-flow$.) The behavior in the Rössler picture (Fig. 7) is exactly the opposite: the system makes a rapid approach to the fixed point. (Note the abrupt "stop" of $z$ as the system it hits the slower sheet of the slow manifold.) The approach to the fixed point in the Rössler model is transverse to the slow manifold, and is therefore fast by definition. This fast approach to the fixed point is fundamentally in conflict with the BZ dynamics.

(ii) The second discrepancy between the BZ dynamics and that of the Rössler picture concerns the funneling of trajectories to the fixed point. This is illustrated in Fig. 8 where, for both systems, we show portions of trajectories starting from three different initial conditions.

For the SNB model [Fig. 8(a)], independently of where trajectories begin, they wrap around the "stable manifold"[30] of the fixed point and are then funneled to the fixed point itself. This wrapping of trajectories produces decaying small oscillations in the time series. For the Rössler picture [Fig. 8(b)] the behavior is quite different: trajectories go directly (vertically) to the slow manifold, showing no affin-

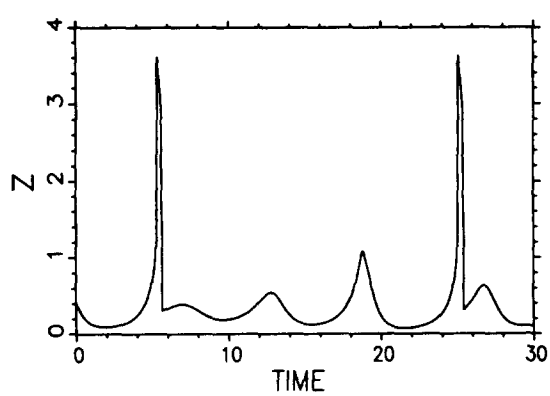


FIG. 7. Time series for the reinjection variable $z$ obtained from the Rössler model with $d = 0.51$ [the same condition as in Fig. 6(d)]. Shown are two relaxation oscillations separated by three small oscillations. The relaxation oscillations show the rapid return of trajectories to the fixed point (lower sheet of the slow manifold).

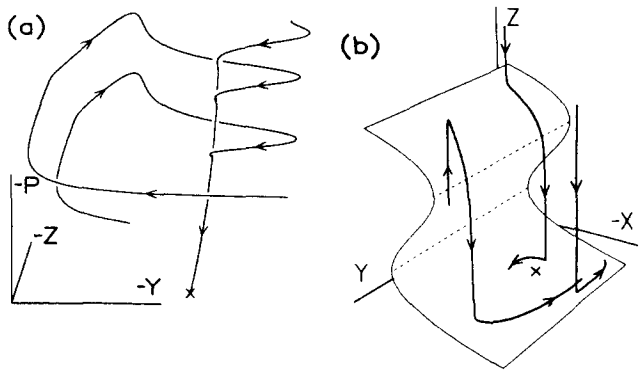


FIG. 8. Transient behavior for both (a) the SNB model and (b) the Rössler model. In each case portions of trajectories are shown starting from three different initial conditions. The parameters for (a) are the same as for Figs. 4 and 5; the parameters for (b) are the same as for Fig. 6(d). For the BZ system (a) trajectories are funneled to the fixed point. This is not the case for the Rössler model (b).

ity for the fixed point. There are no decaying small oscillations in the Rössler model.

(iii) The third point of note is very much related to the previous point and concerns the transition from mixed-mode to small oscillations. In the BZ reaction, preceding the high flow-rate transition to small oscillations, there is a significant range of flow rates for which the spiral lies very close to the fixed point. In this parameter range, the reinjection always brings the system very close to the fixed point and the small oscillations of the mixed-mode state grow from nearly zero amplitude [see Fig. 2(b) and the enlargement in Fig. 4]. This nearly homoclinic condition just before the transition to small oscillations is a very robust feature of the BZ system. It has been observed in experiments,[6,27,28] and simulations[24,28] with control parameters different from those discussed here (see also Larter *et al.*,[31] Albahadily and Schell,[32] and Argoul *et al.*[33])

The situation is different for the Rössler model: there is no mechanism causing the spiral to come close to the fixed point. For the parameter values used to generate Fig. 6, the steady state lies approximately under the upper pleat, so that after the transition to mixed-mode behavior, trajectories come close to the fixed point. However, this is not *robust*—with a different choice of parameters the transition will not be to a nearly homoclinic spiral.

In Fig. 9 we show the situation after the transition to mixed-mode behavior in the Rössler model at parameter values different from those of Fig. 6. Specifically, we have changed $l$ to 0.8 and $d$ to 0.41; all other parameters are given by Eqs. (3). Because the slow manifold depends only on the parameters $a$, $b$, and $c$ [Eq. (4)] and these are unchanged from Fig. 6, the pleats of the slow manifold are unmoved. The position of the fixed point has changed considerably, however, and it no longer lies directly under the upper pleat. Because there is no correlation between the location of the upper pleat and the fixed point, spirals like that shown in Fig. 9 can easily be found after the transition to mixed-mode oscillations in the Rössler model. This is very different from the BZ system.

From the above three discrepancies we conclude that the Rössler model provides an incorrect description of the BZ dynamics. There is an S-shaped manifold giving rise to the variety of the states in the BZ system; however, it is not oriented as in the Rössler picture. This is the subject of Sec. V. However, before turning to this we examine a different model, the hysteresis-Hopf normal form. The slow manifold arising in the normal form is basically of the Rössler type, but its shape is significantly different from that of more traditional Rössler models (e.g., the Gaspard–Nicolis equations) and this has never been stressed.

## IV. THE HYSTERESIS-HOPF NORMAL FORM

The hysteresis-Hopf normal form (HHNF) is a reduced system of equations describing the dynamics found in the vicinity of a hysteresis-Hopf bifurcation. (See Guckenheimer and Holmes[19] for a general discussion of normal forms, and Richetti *et al.*[34] and Barkley *et al.*[24] for a discussion of the HHNF in the context of the BZ reaction.) Our purpose here is to use the normal form only as a slow-manifold model and contrast its dynamics with that of the BZ reaction.

The normal form is given by the following system of equations[35]:

$$\dot{x} = x(z-\beta) - \omega y, \quad \dot{y} = \omega x + y(z-\beta),$$

$$\dot{z} = \frac{1}{\epsilon}\{\lambda + \alpha z - z^3/3 + (x^2+y^2)(b+qx+ez)\},$$

where $\alpha, \beta$, and $\lambda$ are bifurcation parameters, and $\omega, b, q, e, \epsilon$ are nonzero constants.[36] We have added the parameter $\epsilon$ to make the correspondence with other slow-manifold models more transparent. This redundant parameter can be removed by rescaling $z$ and time.

For $q = 0$, the normal form can be transformed into cylindrical coordinates as

$$\dot{r} = r(z-\beta)$$

$$\dot{\theta} = \omega$$

$$\dot{z} = \frac{1}{\epsilon}\{\lambda + \alpha z - z^3/3 + r^2(b+ez)\}$$

which, for $\epsilon$ small, has a slow manifold given by

$$r^2 = (z^3/3 - \alpha z - \lambda)/(b+ez).$$

For appropriate choices of parameters, this manifold has an hourglass shape. With $q$ nonzero the hourglass is no longer axisymmetric. Figure 10 shows a cutaway of the slow manifold at two values of $\lambda$ with $q$ nonzero. The parameters values are

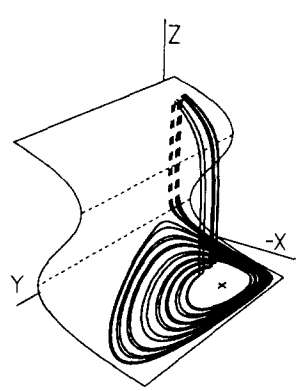


FIG. 9. Results from the Rössler model [Eqs. (2)] with $l = 0.8$, $d = 0.41$, and other parameters given by Eqs. (3). The state shown occurs after the transition to mixed-model behavior, yet the reinjection does not bring trajectories close to the fixed point.

$$\alpha = 1.0, \beta = 0.5, \omega = 40,$$
$$b = -5.0, e = 2.0, q = -0.8, \epsilon = 1 \times 10^{-2}. \quad (5)$$

In relation to the BZ dynamics, the significant improvement of the HHNF over the Rössler model is that the hourglass shape of the slow manifold in the normal form causes trajectories to be funneled into a thin tube and then to the fixed point itself. Compare Fig. 10(a) for the HHNF with Fig. 5 for the SNB model, and note that decaying small oscillations are found in both. Contrast this behavior with that of the Rössler picture shown in Fig. 6.

Still, major differences exist between the HHNF and BZ dynamics. Most notably, the time dependence of the reinjection variable $z$ in the normal form is contrary to that of the reinjection variable $P$ in the SNB model: in the HHNF trajectories approach the saddle-focus transverse to the slow manifold, and thus with a fast time scale (rather than a slow time scale as in the BZ system). Point (i) of Sec. III C therefore applies to the normal form as well as to the more traditional Rössler model.

Shown in Fig. 11 is a time series for the variable $z$ in the normal form. The rapid jumps between sheets of the slow manifold are clearly seen. It is important to note that while this time series bears resemblance to time series obtained for the BZ reaction (both experiments and simulations), this resemblance is misleading. Figure 11 is a plot of the reinjection variable; the time series it resembles in the BZ system are for the concentrations of $Br^-$ or $Ce^{4+}$, and these are not the reinjection variable.

The other important differences between the HHNF and BZ dynamics concern the funneling of trajectories. First, although trajectories in the HHNF are funneled to a narrow tube, this funneling is quite different from the funneling in the BZ system. It is clear that in the normal form (Fig. 10), all trajectories spiral inward to a thin tube at the same distance from the saddle-focus fixed point. In the SNB model, however, trajectories starting from different initial conditions spiral inward at different distances from the fixed point [Fig. 8(a)].

Second, in the HHNF, the funneling of trajectories and the decaying small oscillations are associated with a "virtual pair" of fixed points. While it is tempting to also associate the decaying small oscillations in the BZ system with a virtual pair of fixed points, we find that this cannot be done in general.

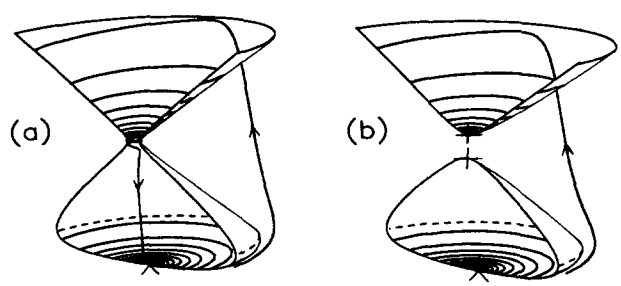


FIG. 10. Cutaway of the slow manifold in the hysteresis-Hopf normal form: (a) $\lambda = 0.68$; (b) $\lambda = 0.60$. For clarity the coordinate axes are not shown; the slices are at $x = 0$, and $z$ is increasing *downward*. Also shown are fixed points and illustrative trajectories. The $\times$'s at the bottom of the figures correspond to the saddle-focus fixed points previously discussed in the BZ and Rössler systems. The $+$'s in (b) mark two fixed points which arise by a saddle-node bifurcation at $\lambda = 2/3$; the upper (middle) fixed point is stable (unstable). It is meaningful to associate the contracting spiral in (a) with the pair of fixed points which appear in (b).

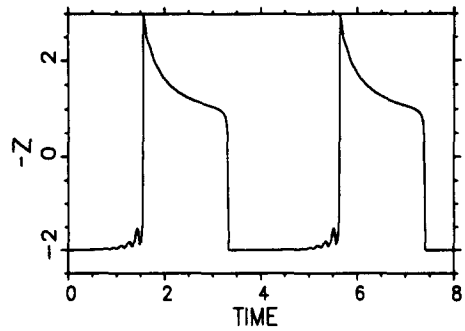


FIG. 11. Time series for the reinjection variable $z$ in hysteresis-Hopf normal form. Parameter values are those of Fig. 10(a). Note that trajectories spend a long time passing through the neck of the hourglass in Fig. 10(a).

More specifically, in the normal form, trajectories are funneled to a thin tube only when the neck of the hourglass is very narrow [(Fig. 10(a)]. But then, for a slight change of parameters, the neck pinches off, resulting in a saddle-node bifurcation. The two new fixed points [Fig. 10(b)] have complex conjugate eigenvalues with negative real part; the upper (middle) fixed point is stable (unstable). The dynamics in the nonbifurcating directions $x$ and $y$, is approximately the same in both (a) and (b); trajectories spiral inward. Thus, *for the normal form*, it is appropriate to associate the decaying small oscillations at the top of Fig. 10(a) with a virtual pair of fixed point which become actual fixed points in Fig. 10(b).

This simple picture does not apply to the BZ system. Referring back to the time series (Fig. 4) and phase portrait (Fig. 5) for the SNB model, we see that the reinjection variable $P$ changes very rapidly throughout the decay of small oscillations. The decaying oscillations are found just after $-\log P$ reaches a maximum and begins to decrease; however, from the time series, after $\dot{P}$ changes sign, $-\log P$ decreases very rapidly.

Contrast this with the behavior in the HHNF (Figs. 10 and 11): the reinjection variable $z$ slows down as the system passes through the neck of the hourglass. Thus, trajectories spend a long time in the region of phase space where the funneling occurs. Using a funneling mechanism like that illustrated in Fig. 10, one would have to be *exceedingly* close to a saddle-node bifurcation to get small oscillations to decay to the extent that they do in the BZ system [Figs. 2(b), 4, and 5].

Finally, it has been our observation that, *in the SNB model*, saddle-node bifurcations generally occur away from the decaying small oscillations. This is illustrated in Fig. 12. The plus sign shows a typically located saddle node on the BZ spiral. For larger flow rates a pair of fixed points merges from this saddle node. Each fixed point has all real eigenvalues. It is easy to verify that such a bifurcation is not possible in the hysteresis-Hopf normal form.[24]

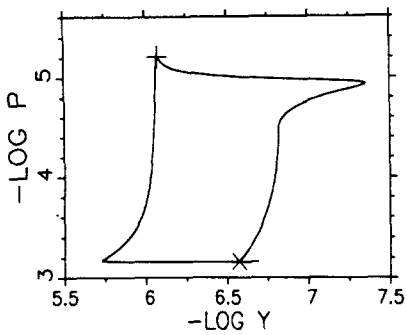


FIG. 12. Phase portrait from the SNB model showing the location of a saddle node (marked by + ) on the spiral attractor. As before the saddle focus is marked by an ×. The parameter values are given by Eqs. (1) except that $k_0 = 2.035\times10^{-2}\,s^{-1}$, and $Y_0 = 2.2\times10^{-6}$ M.

## V. THE BOISSONADE PICTURE

We now turn to a slow-manifold model which overcomes the failures of the Rössler model and hysteresis-Hopf normal form, and which exhibits mixed-mode oscillations like those seen in the BZ system. We have independently developed a model that provides an illustration of a class of models which we collectively refer to as the Boissonade type. We refer to our model as model A. While many researchers have developed models along similar lines,[2,5,7,8,37–44] Boissonade was the first to recognize the important process that gives rise to mixed-mode oscillations in chemical reactions.

### A. Model A

We begin by presenting model A in very general terms. (Below we present a system of equations which makes the model precise.) Consider first two systems, which we denote I and II, whose properties are illustrated in Fig. 13. For system I we show a bifurcation diagram; $A$ and $B$ represent state variables, and $\beta$ represents a control parameter. As $\beta$ is decreased the system undergoes a Hopf bifurcation to nearly harmonic oscillations. This is the only property of I essential to the generation of mixed-mode oscillations in model A. The effect of terminating the oscillations in I at low values of $\beta$ will be discussed below.

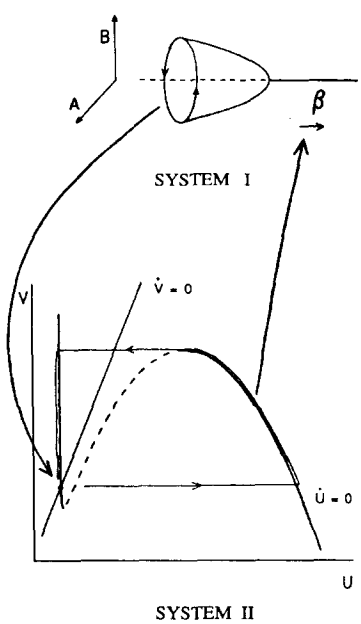


FIG. 13. Schematic diagram of model A. For system I, a bifurcation diagram is shown for a two-variable system exhibiting a Hopf bifurcation. For system II, the nullclines of a two-variable slow-manifold model are shown; the trajectory illustrates the evolution after a sufficiently large perturbation of the excitable fixed point. Model A is formed by coupling systems I and II: the nearly harmonic oscillations in I perturb the excitable fixed point in II, and the relaxation oscillations in II increase the effective bifurcation parameter in I.

System II is a two-variable system whose nullclines ($\dot U = 0$, $\dot V = 0$) are as shown. Trajectories are attracted to the solid portion of the $U$ nullcline much faster than they are attracted to the $V$ nullcline. The behavior of such a system is well known[2,4,10,45] depending upon where the nullclines intersect, the system will exhibit either relaxation oscillations or an excitable steady state. We illustrate the excitable case in Fig. 13. For small pertubations of the fixed point, the system returns directly to the fixed point. For larger perturbations, the system undergoes a large excursion (as shown) before returning to the steady state.

Model A consists of systems I and II coupled as shown schematically in Fig. 13. The small-amplitude oscillations of I perturb the fixed point of II. The instantaneous value of the variable $V$ in II influences the effective bifurcation parameter for I. Specifically, an increase in $V$ raises the value of $\beta$ seen by I.

We assume that the time scale for the variable $U$ is much faster than that of the other three variables. Thus the slow manifold in model A is the $U$ nullcline. Figure 14 shows a sketch of a spiral attractor for our (four-dimensional) model projected onto a three-dimensional subspace. The $U$ nullcline, itself three dimensional, is seen as two dimensional in the projection. We illustrate the model A spiral with a sketch because the actual small oscillations of the spiral are too small to be visible on the scale of the slow manifold (see Fig. 16 below).

The essential feature of our model, and all models of the Boissonade type, is that a relaxation oscillation in one system (II), drives another system (I) back and forth across a Hopf bifurcation. The slow manifold arises in connection with the relaxation oscillations. There have been many variations on this theme. Chemical feedback or coupling between component systems has most often been studied.[2,5,7,8,37–39,42–44] Various physical couplings have also been considered.[2,40,41,44] In many of these studies the Hopf bifurcation is subcritical. (See Baer *et al.*[46] for a general discussion of slow passage through a Hopf bifurcation.)

As will be seen, the influence of system II on system I is primarily responsible for generating the spiral attractor. Such a coupling is also very natural from a chemical point of view. Consider $\beta$ as the feed concentration of chemical species $A$ in a CSTR. Then virtually any reaction which produces $A$ from $V$ (e.g., $V\rightarrow A$) will provide the desired coupling: an increase in $V$ will increase the effective feed of $A$.

The exact form of the influence of system I on system II is probably important for detailed modeling of the BZ reac-

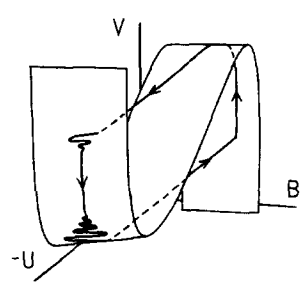


FIG. 14. Projection of the slow manifold for model A onto a three-dimensional subspace, together with a sketch of a spiral attractor on this manifold. The axes are not centered on the origin, and the $U$-axis points in the direction of decreasing $U$. At large values of $V$, the small oscillations decay; as $V$ decreases the effective bifurcation parameter in system I crosses the Hopf bifurcation and growing small oscillations appear.

tion; however, we have investigated different couplings and have found that the generation of mixed-mode oscillations are largely insensitive to its details. From a chemical point of view, this means that many reactions can provide an appropriate coupling of the two systems. For model A we choose a coupling which generates a simple slow manifold: we let the variable $B$ in system I perturb the variable $V$ in system II.

We shall not present a kinetic scheme to model the above systems, rather we simply use known differential equations arising from chemical models to derive a system of differential equations which describes the coupled system. We shall use the model studied by Gray and Scott[47] as an example of system I, and the model studied by Tyson and Fife[45] as an example of system II.[48]

The differential equations for the Gray–Scott system are

$$\dot{A} = -AB^2 - k_0(A - A_0),$$
$$\dot{B} = AB^2 - k_1 B - k_0(B - B_0),$$

and those of the Tyson–Fife system are

$$\dot{U} = \frac{1}{\epsilon}\left\{U(1-U) - bV\left(\frac{U-a}{U+a}\right)\right\},$$
$$\dot{V} = U - V.$$

We couple these systems by introducing the coupling constants $g_1$ and $g_2$, and a constant $k$ to adjust the relative timescales of the subsystems. We obtain

$$\dot{A} = -AB^2 - \alpha A + g_1 V + \beta,$$
$$\dot{B} = AB^2 - \gamma B + \delta,$$
$$\dot{U} = \frac{k}{\epsilon}\left\{U(1-U) - b(V + g_2 B)\left(\frac{U-a}{U+a}\right)\right\}, \qquad (6)$$
$$\dot{V} = k(U - V - g_2 B),$$

where we have made the obvious redefinitions of parameters. The couplings are as advertised: $g_1 V$ serves the same role as $\beta$ ($\beta = k_0 A_0$), and $g_2 B$ perturbs the value of $V$.

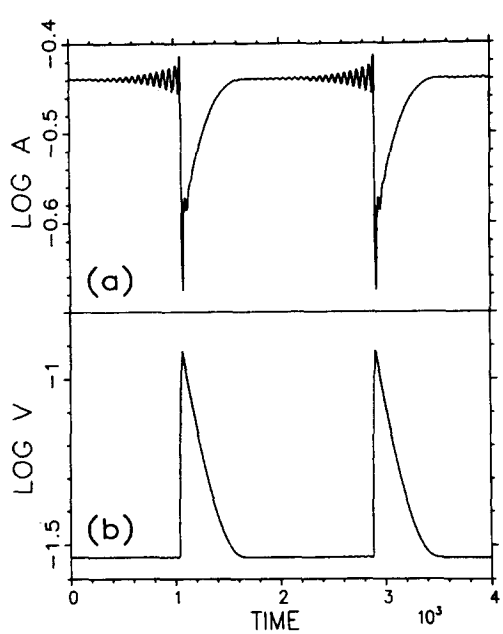


FIG. 15. Mixed-mode oscillations obtained from model A: $\beta = 3.0\times10^{-2}$.

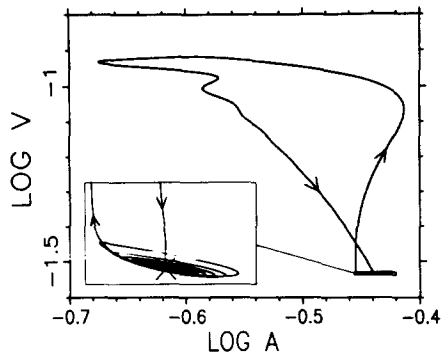


FIG. 16. Phase portrait of the mixed-mode state shown in Fig. 15. The enlargement shows the small oscillations and the saddle-focus fixed point (marked with an $\times$).

### B. Results

We now present results obtained by numerically integrating model Eqs. (6). The results presented in this section concern the mixed-mode oscillations observed at high flow rates in the BZ reaction; the Appendix contains a variety of other states of interest. Unless stated otherwise, the model parameters are assigned the following values throughout:

$$\alpha = 10^{-3},\ \gamma = 0.12,\ \delta = 2.0\times10^{-3},$$
$$a = 10^{-2},\ b = 2.5,\ k = 5.0\times10^{-3},$$
$$g_1 = 0.2,\ g_2 = -2.0\times10^{-2},\ \epsilon = 10^{-3}. \qquad (7)$$

In Fig. 15 and 16 we show a time series and phase portrait at $\beta = 3.0\times10^{-2}$. Figure 17 provides a summary of states as a function of $\beta$. The similarity between the model dynamics and that seen in the BZ system is striking [cf. experiment (Figs. 2 and 3) and simulation (Figs. 4 and 5)]. Note, however, that Fig. 17 is somewhat misleading in that the vertical scale changes as a function of $\beta$; the mixed-mode oscillations at high $\beta$ are of smaller amplitude in A than those at low $\beta$.

Referring to Figs. 13–15, we see that mixed-mode behavior occurs naturally in model A as follows: consider system II initially near steady state and the amplitude of the small oscillations in system I increasing ($time = 2\times10^3$ in Fig. 15). Eventually, due to the perturbation of I on II, system II is driven to make a large relaxation oscillation ($time \approx 2.9\times10^3$). The resulting increase in $V$ causes the effective value of $\beta$ to increase past the Hopf bifurcations in system I and this brings about the decay of small-amplitude oscillations ($time \approx 3\times10^3$). Then, as $V$ relaxes back to its "steady state" value, $\beta$ decreases back through the Hopf bifurcation and small oscillations return (from almost zero amplitude). The process then repeats.

The transition from steady state to mixed-mode oscillations at large $\beta$ (Fig. 17, $3.0\times10^{-2} \leqslant \beta \leqslant 3.2\times10^{-2}$), occurs essentially in the way put forth by Schmitz *et al.*[3] At large values of $\beta$, system I has a stable steady state, and so too with the coupled system. As $\beta$ is decreased, a Hopf bifurcation occurs in I giving rise to small oscillations. At some value of $\beta$ the amplitude of the small oscillations becomes large enough to perturb II into its relaxation mode, thus bringing about the transition to the spiral state. (We say more about this transition in Sec. VI.) Just as in the Rössler picture, as $\beta$

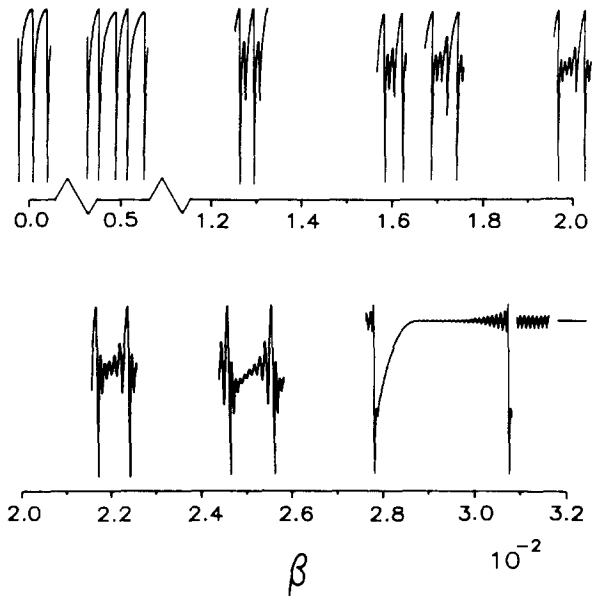


FIG. 17. Summary of states observed in model A as a function of the control parameter $\beta$. Representative time series (log A vs *time*) are shown at several values of $\beta$. The vertical scale changes as a function of $\beta$: the states at low $\beta$ are of greater amplitude than those at high $\beta$.

is decreased further the ratio of large to small oscillations increases until only large oscillations are found.

Ultimately, as $\beta$ is decreased, there is a hysteretic jump back to steady state. This hysteresis comes about as follows: for the parameter values considered, the oscillations in system I (the Gray–Scott model) terminate, at low values of $\beta$ in a Hopf bifurcation. Below this Hopf bifurcation the steady state in system I is stable, and hence, so is the steady state for the coupled system. Given a sufficiently large perturbation, however, system II will undergo a relaxation oscillation, and this increases the effective bifurcation parameter in system I. If $\beta$ is sufficiently close to the lower Hopf bifurcation, the increase in the effective parameter is such that as II returns to its steady state, the oscillations in I are large enough to perturb II again. Thus, a stable large-amplitude limit cycle can coexist with the steady state stabilized at the lower Hopf bifurcation. From a bifurcation-theoretic point of view, model A has subcritical (though almost degenerate) Hopf bifurcation at $\beta = -8.271 \times 10^{-4}$.

We now note how the Boissonade picture (model A in particular) overcomes the three failures of the Rössler picture discussed in Sec. III C.

(i) The time dependence during the reinjection phase in model A is the same in as in the SNB model [compare Figs. 15(b) and 4(b)]. Specifically, model A shows the same slow approach to the saddle focus as does the BZ system. The reason for this is clear from the slow manifold illustrated in Fig. 14: the system is on the slow manifold as it approaches the fixed point [unlike in the Rössler picture (Fig. 1) where the system approaches the fixed point transverse to the slow manifold].

(ii) In Fig. 18 we show, for model A, portions of trajectories starting at three different initial conditions. Trajectories wrap around the "stable manifold" of the fixed point in much the way they do in the SNB model [Fig. 8(a)]. The reason is as follows: the steady state curve of system I, taken as a function of $V$ rather than of $\beta$, closely approximates the "stable manifold" of the fixed point for model A. For large $V$, the effective value of $\beta$ seen by system I is above the Hopf bifurcation. Thus at large $V$, trajectories in model A spiral into the pseudo-steady state of system I, i.e., the stable manifold of the fixed point.

(iii) The mixed-mode behavior in model A just below the transition to small oscillations (Fig. 17, $\beta = 3.0 \times 10^{-2}$) is the same as in the BZ reaction (Fig. 3, *flow* = 5.37 ml/min). There is a range of control parameter below the transition for which the spiral lies very close to the fixed point. [Compare the phase portraits for the SNB model (Fig. 5) and model A (Fig. 16) and contrast these with the phase portrait for the Rössler model shown in Fig. 9.] We emphasize, as we did for the BZ system (Secs. II and III C), that this is a robust feature of model A. While the spiral we show was chosen because it closely matches that seen in simulations and experiment, similar spirals are extremely common in model A at the transition from mixed-mode to small oscillations.

## VI. DISCUSSION

We proceed with a further examination of model A and note some areas where future work is needed. We focus on six points.

(i) Our method has been to compare the dynamics of experiments and simulations of a chemically based model (SNB) with the dynamics of mathematical models based on slow manifolds. However, one might also take a more direct approach and try to derive an analytic expression (in some approximation) for the slow manifold in the SNB model. We have not succeeded in accomplishing this. (Note that the differential equations for the SNB model have a total of 47 terms and 17 parameters.)

Tyson *et al.*[4,45,49] have derived expressions which approximate slow manifolds in other models of the BZ reaction. In fact, the Tyson–Fife equations which we have incorporated into model A represent a slow-variable reduction of the irreversible Oregonator model.[15] However, these expressions give an inadequate approximation to the slow manifold in the SNB model (note Ref. 48). This is simply because, in the SNB model, HOBr( = P) is the reinjection variable, but this variable plays no role in the irreversible Oregonator. Thus no reduction of the irreversible Oregonator can give a

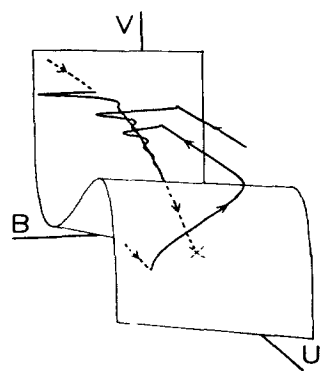


FIG. 18. Transients for model A. Trajectories are shown starting from three initial conditions. The parameters are the same as those of Figs. 15 and 16. The view is from positive $U$ and shows the side of the slow-manifold opposite that of Fig. 14. As in the BZ system, trajectories are funneled to the fixed point (marked by an $\times$).

slow manifold with P as the reinjection variable. In the analysis of Tyson and Fife, $V$ is proportional to the concentration of $Ce^{4+}$; in the SNB model, however, the dynamics of $Ce^{4+}$ ( = Z) is very similar to that of $Br^-$ ( = Y).

Turner[5] has studied a reversible model treating $P$ as a slow variable. Janz *et al.*,[7] Rinzel and Troy,[8,38] have studied bursting in the irreversible Oregonator with the stoichiometric factor $f$ parameterized by $P$. Still, we know of no analytic expression for the slow manifold in the SNB, or any other model, having $P$ as the reinjection variable. Such an expression would clearly be of great value.

(ii) While the sequence of states for model A (Fig. 17), closely resembles that of experiment (Fig. 3), the model sequence does not have the chaotic regions reported in experiment. (A similar absence of chaos was also noted for the SNB model in Sec. II B.) For model A, the sequence contains period doublings, but apparently no full cascade to chaos. Also found are partial Farey sequences, that is, a few concatenations of patterns.[50] The transitions between periodic states with different patterns are often hysteretic.

Note, however, that it is not hard to find chaos in model A (see the Appendix, Fig. 20). Still we have not been able to exactly match the experiments of Hudson *et al.* Specifically, we have not found a sequence which simultaneously shows chaos and a spiral lying close to a saddle-focus. Whether or not this is fundamental to the Boissonade picture needs further investigation.

(iii) It is of interest that models of the Boissonade type lead naturally to Šilnikov spirals (i.e., spiral attractors lying near saddle-focus fixed points), and that these models generate nearly homoclinic spirals over a range of parameters values. While this "persistent homoclinicity" is common at high flow rates in the BZ system, it is not common in the Rössler models which have been used to investigate homoclinic behavior.[29,51,52] Bifurcation diagrams for models of the Boissonade type are undoubtedly different from those typically associated with Šilnikov behavior. This point needs much further study.

(iv) We note that simulations[34] of the hysteresis-Hopf normal form have produced mixed-mode states resembling those seen in experiments.[53] Simulations of a different model (also of the Rössler type) have yielded dynamics which compare very well with experiment.[9] In this latter case, Argoul *et al.* have interpreted experimental observations of chaos in the BZ reaction as arising from nearly homoclinic conditions.

While the analysis of Argoul *et al.* regarding the proximity to homoclinicity is undoubtedly correct, the mechanism giving rise to the homoclinicity is probably not as they assumed. In fact, their experimental data provides an excellent illustration of the differences between slow manifolds of Rössler and Boissonade types. Specifically, the experimental phase portrait in Fig. 1(b) of Argoul *et al.*[9] is very similar to those of model A (Figs. 16 and 18). It is apparent that the experimental trajectory strikes a slow manifold and then undergoes decaying small oscillations as it approaches the (assumed) fixed point. Thus, while their simulations compare favorably with experiment, the reinjection mechanism of their model is probably not correct. It would be of interest to estimate the relative eigenvalues of the fixed point directly from the experimental data, and also to see if model A can reproduce the dynamics reported in these experiments.

(v) Model A necessarily requires a four-dimensional state space. This is as follows: because orbits cannot intersect, the dynamics shown in the phase portrait enlargement (Fig. 16), and transient plot (Fig. 18), for model A requires at least three dimensions [see also Figs. 5 and 8(a) for the SNB model]. *But these dynamics take place on the slow manifold.* Because the dimension of the full state space must be at least one greater than that of the slow manifold, the state space must be at least four dimensional.

This would suggest a reason why complex oscillations have never been observed in the three-variable simple Oregonator model (SOM) of Field and Noyes[15]: there simply are not enough variables. The SOM represents too drastic a reduction of the mechanism of the BZ reaction. The SOM has an S-shaped slow manifold and correspondingly it exhibits relaxation oscillations; however, because there is no possibility of complex dynamics occurring within the slow manifold itself, there is no possibility for the SOM to show the kind of mixed-mode behavior which we have examined here. It is possible, however, that with parameters such that time scales become comparable, the SOM shows complex dynamics, i.e., chaos. (Of course there are other three variable models exhibiting complex dynamics, e.g., the model analyzed by Rinzel and Troy.[8])

(vi) Finally, we discuss the two most notable the shortcomings of model A. The first is the virtual absence of supercritical secondary-Hopf bifurcations between the small and mixed-mode oscillations. In the SNB model, secondary-Hopf bifurcations, and hence tori, are often found at the transition from mixed-mode to small oscillations.[24] While Hudson *et al.*[13] do not show a torus in their experimental diagram (Fig. 3), they report oscillations between the small and mixed-mode oscillations which undoubtedly lie on a torus. In model A, however, the transition to mixed-mode oscillations almost always occurs via either period-doubling or subcritical secondary-Hopf bifurcations. For the sequence of model states shown in Fig. 17, the transition occurs after a period doubling of the small oscillations (we have not resolved the details of the transition). An extensive search has revealed supercritical secondary-Hopf bifurcations in model A, but these occur far too infrequently to account for the tori seen in the BZ system.

It is possible that a different coupling of the two component systems of model A would solve this problem. We have briefly explored a few variations in the way system I perturbs system II, but to no avail. We now feel that the absence of tori reflects a more fundamental insufficiency of our model. Improvement of model A could probably come by incorporating slow-manifold models different from those considered here (e.g., those reviewed by Rinzel[11]).

The second major shortcoming of model A is that the steady-state structure of the model is different from that of the SNB model. Specifically, it is possible to find fixed points in model A with *four unstable directions* (eigenvectors). This is expected because each of the components systems, I and II, can independently exhibit Hopf bifurcations. How-

ever, to our knowledge, no one has ever observed a steady state in a chemical model of the BZ reaction which has more than *two unstable directions*. Ringland[28] was unable to find such fixed points in the SNB model after many systematic attempts. We believe that this limitation of steady states of two unstable directions is a fundamental part of the BZ dynamics, yet model A fails to capture this feature. It would be of great interest to have a simple geometrical model which reflected this interesting steady-state character of the BZ system.

## VII. CONCLUSION

We have examined the mixed-mode oscillations in the BZ reaction with an eye to understanding the slow-manifold picture which explains them. We have extensively contrasted the dynamics found in the BZ system with the dynamics found in models of the type originally proposed by Rössler. We have developed a simple slow-manifold model (model A) of the type first proposed by Boissonade. This model is based on the coupling of two very simple systems. We have shown that model A naturally reproduces most of the dynamics observed at high flow rates in the BZ reaction.

While we have focused on mixed-mode oscillations in the BZ reaction, many other systems show similar complex oscillations.[31,32,39,40,54] In some cases, the observed oscillations are also understood in terms of the coupling (chemical or physical) of oscillators. Therefore our analysis of the fundamental differences between slow-manifold models is applicable to these systems as well. We, in fact, feel that the Rössler slow-manifold picture illustrated in the introduction (Fig. 1), is unlikely to account for the mixed-mode oscillations in any homogeneous chemical system; models of the Boissonade type are much more appropriate for complex chemical reactions.

Finally, we note that there are some features of the BZ dynamics that our simple model fails to capture; in particular, the details of the transition from small to mixed-mode oscillations are lacking. Thus there is a need for further development of simple geometrical models for the dynamics of the BZ reaction.

## ACKNOWLEDGMENTS

I wish to thank Richard Field, John Rinzel, and Laurette Tuckerman for very helpful discussions. This work was partially supported by the Department of Energy Office of Basic Energy Sciences. The computations were performed at the University of Texas Center for High Performance Computing.

## APPENDIX

In this Appendix we present interesting dynamics found in model A. We focus on three of the most important types of behavior in the BZ reaction: quasiperiodicity, chaos, multipeaked periodicity (i.e., Farey sequences). Only those parameter values different from Eqs. (7) are given.

Figure 19 shows a time series and phase portrait for a quasiperiodic state, i.e., a two torus. This state is quite similar to that observed in the Bordeaux experiments[33,55] and in simulations of the SNB model.[24]

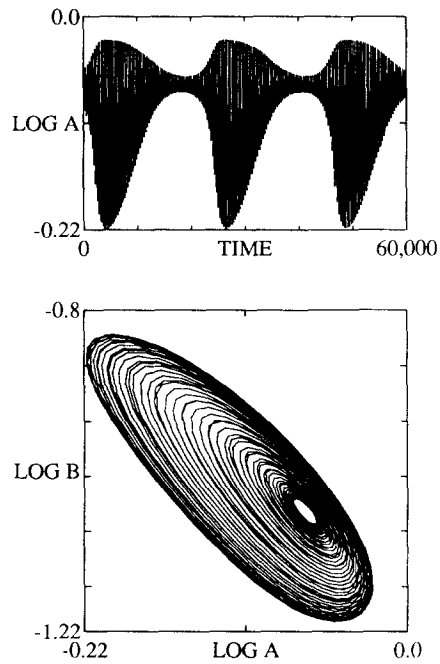


FIG. 19. Time series and phase portrait for a quasiperiodic state, i.e., a two torus. Parameters: $\alpha = 2.0\times10^{-2}$, $\beta = -1.5084\times10^{-2}$, $\delta = 4.0\times10^{-3}$, $b = 2.4$, $k = 10^{-5}$, $g_1 = 2.0$, $g_2 = 0.05$, $\epsilon = 10^{-2}$.

Figure 20 shows a time series and phase portrait for a chaotic state. This state is a chaotic mixture of two patterns: one large four small and one large five small [$C_5$ in the notation originally used by the Texas group,[56] $C_1^{4,5}$ in the Bordeaux notation.[33]] The phase portrait shows 10 000 time units (though we have integrated over a much longer time

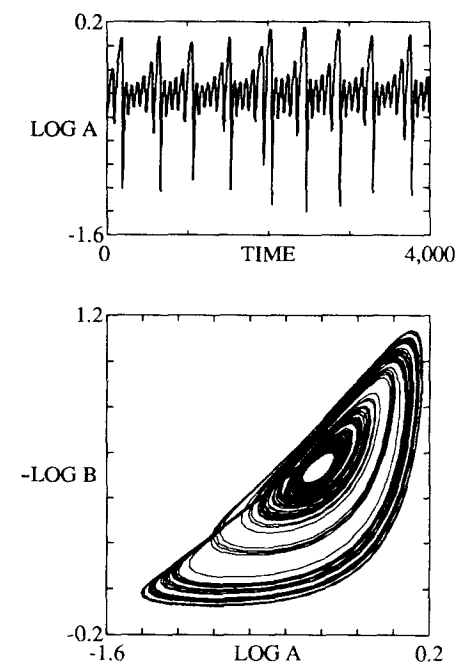


FIG. 20. Time series and phase portrait for a chaotic state. Parameters: $\alpha = 2.0\times10^{-2}$, $\beta = 3.6\times10^{-2}$, $g_1 = 0.1$, $g_2 = 4.0\times10^{-2}$.

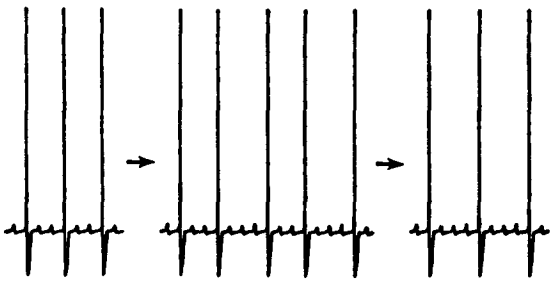

FIG. 21. Three multipeaked-periodic states illustrating concatenation of patterns, that is, Farey sequences. Parameters: $\alpha = 0.02$, $k = 0.1$, $g_1 = 0.1$, $g_2 = -5.0\times10^{-3}$, and from left to right: $\beta = 3.734\times10^{-2}$, $3.7365\times10^{-2}$, and $3.738\times10^{-2}$.

and not observed the system to repeat). In the phase portrait, $-\log B$ is plotted to emphasize the similarity to the *Texattractor*.[56,57] Note that the parameters are not very different from those of Fig. 17 for which no chaos was found. This state represents bands on a wrinkled torus [e.g., Ref. 24, Fig. 8(c)].

Figure 21 shows three multipeaked-periodic states illustrating concatenation of patterns (Farey sequences). Shown are time series ($\log U$ vs time) ordered as a function of control parameter $\beta$. Between the two relatively simple parent states is found the daughter whose pattern is the concatenations of those of the parents. In the two gaps between these states are many more (perhaps infinitely many) periodic states ordered by this rule. Compare with experiment[50] and simulations.[31] See Barkley[58] for an explanation of these sequences.


[1]O. E. Rössler, Z. Naturforsch. Teil A **31**, 259, 1664 (1976); Bull. Math. Biol. **39**, 275 (1977).
[2]J. Boissonade, J. Chim. Phys. **73**, 540 (1976).
[3]R. A. Schmitz, K. R. Graziani, and J. L. Hudson, J. Chem. Phys. **67**, 3040 (1977).
[4]J. J. Tyson, J. Chem. Phys. **66**, 905 (1977); J. Math. Biol. **5**, 351 (1978).
[5]J. S. Turner, Discussion Meeting, Kinetics of Physico–Chemical Oscillations, Aachen, 1979, p. 61.
[6]J. Maselko, Chem. Phys. **51**, 473 (1980).
[7]R. D. Janz, D. J. Vanecek, and R. J. Field, J. Chem. Phys. **73**, 3132 (1980).
[8]J. Rinzel and W. C. Troy, J. Chem. Phys. **76**, 1775 (1982).
[9]F. Argoul, A. Arneodo, and P. Richetti, Phys. Lett. A **201**, 269 (1987).
[10]P. DeKepper and J. Boissonade, in *Oscillations and Traveling Waves in Chemical Systems*, edited by R. J. Field and M. Burger (Wiley, New York, 1985), p. 223.
[11]J. Rinzel, in *Lecture Notes in Biomathematics*, edited by E. Teramoto and M. Yamaguti (Springer, New York, 1987), Vol. 71, p. 267.
[12]K. Showalter, R. M. Noyes, and K. Bar-Eli, J. Chem. Phys. **69**, 2514 (1978).
[13]J. L. Hudson, M. Hart, and D. Marinko, J. Chem. Phys. **71**, 1601 (1979).
[14]J. L. Hudson, D. Marinko, and C. Dove, Discussion Meeting, Kinetics of Physico–Chemical Oscillations, Aachen, 1979, p. 71.
[15]R. J. Field and R. M. Noyes, J. Chem. Phys. **60**, 1877 (1974).
[16]IMSL Library manual, 7th ed. (IMSL, Houston, 1979).
[17]A point which has often been overlooked in the comparison of model and experiment concerns the response of the bromide ion electrodes used to make measurements. While the output potential of these electrodes depends in a complicated way on the concentration of $Br^-$ as well as other species (and on the their time evolution), it is clear that *lower* bromide ion concentrations correspond to *larger* output potentials of the electrode and *vice versa*. We use the simplest approximation to the electrode response and plot $-\log[Br^-]$. This approximation is not valid at low $Br^-$ concentrations; the sharp (low $[Br^-]$) spike in Fig. 4 could not be detected by a bromide-ion electrode.
[18]L. P. Šilnikov, Sov. Math. Dokl. **6**, 163 (1965).
[19]J. Guckenheimer and P. Holmes, *Nonlinear Oscillations, Dynamical Systems and Bifurcations of Vector Fields* (Springer, New York, 1984).
[20]N. Ganapathisubramanian and R. M. Noyes, J. Chem. Phys. **76**, 1770 (1982).
[21]J. Rinzel and I. B. Schwartz, J. Chem. Phys. **80**, 5610 (1984).
[22]R. M. Noyes, in *Stochastic Phenomena and Chaotic Behavior in Complex Systems*, edited by P. Schulster (Springer, Berlin, 1984), p. 107.
[23]D. Lindberg, Ph. D. thesis, University of Texas, Austin, Texas (1988).
[24]D. Barkley, J. Ringland, and J. S. Turner, J. Chem. Phys. **87**, 3812 (1987).
[25]J. C. Roux, Physica D **7**, 57 (1983).
[26]H. L. Swinney and J. C. Roux, in *Non-Equilibrium Dynamics in Chemical Systems*, edited by C. Vidal and A. Pacault (Springer, New York, 1984), p. 124.
[27]M. H. Kilgore, Ph. D. thesis, University of Texas, Austin, Texas (1986).
[28]J. Ringland, Ph. D. thesis, University of Texas, Austin, Texas (1986).
[29]P. Gaspard and G. Nicolis, J. Stat. Phys. **31**, 499 (1983).
[30]We use the term stable manifold loosely here; we mean the one-dimensional curve along which trajectories approach the saddle-focus fixed point.
[31]R. Larter, C. L. Bush, T. R. Lonis, and B. D. Aguda, J. Chem. Phys. **87**, 5765 (1987).
[32]F. N. Albahadily and M. Schell, J. Chem. Phys. **88**, 4312 (1988).
[33]F. Argoul, A. Arneodo, P. Richetti, and J. C. Roux, J. Chem. Phys. **86**, 3325 (1987).
[34]P. Richetti, J. C. Roux, F. Argoul, and A. Arneodo, J. Chem. Phys. **86**, 3339 (1987).
[35]W. F. Langford, SIAM J. Appl. Math. **37**, 22 (1979); *Nonlinear Dynamics and Turbulence*, edited by G. I. Barenblatt, G. Iooss, and D. D. Joseph (Pitman, Boston, 1982), p. 215.
[36]The parameter $q$ does not come from the normal form reduction, but was added by Langford to break the axisymmetry of the normal form.
[37]J. J. Tyson, J. Chem. Phys. **58**, 3919 (1973).
[38]W. C. Troy, in *Oscillations and Traveling Waves in Chemical Systems*, edited by R. J. Field and M. Burger (Wiley, New York, 1985), p. 145.
[39]J. Maselko, M. Alamgir, and I. R. Epstein, Physica D **19**, 153 (1986).
[40]M. Schell and J. Ross, J. Chem. Phys. **85**, 6489 (1986).
[41]M. F. Crowley and R. F. Field, J. Phys. Chem. **90**, 1907 (1986), *Lecture Notes in Biomathematics*, edited by H. Othmer (Springer, New York, 1986), Vol. 66, p. 68.
[42]Z. Noszticzius, W. D. McCormick, H. L. Swinney, and Z. A. Schelly, Acta Polytech. Scand. **178**, 57 (1987).
[43]O. Citri and I. R. Epstein, J. Phys. Chem. **92**, 865 (1988).
[44]L. Gyorgyi and R. J. Field, J. Chem. Phys. (to be published).
[45]J. J. Tyson and P. C. Fife, J. Chem. Phys. **73**, 2224 (1980).
[46]S. M. Baer, T. Erneux, and J. Rinzel, SIAM J. Appl. Math. (to be published).
[47]P. Gray and S. K. Scott, Chem. Eng. Sci. **38**, 29 (1983).
[48]We stress that we use the Tyson–Fife equations only as mathematical model exhibiting the dynamics of interest (that is the dynamics of system II); we in no way intend to associate the original chemical species of the Tyson–Fife model with the *same species* in the BZ reaction.
[49]J. J. Tyson, J. Phys. Chem. **86**, 3006 (1982).
[50]J. Maselko and H. L. Swinney, Phys. Scr. **T9**, 35 (1985); J. Chem. Phys. **85**, 6430 (1986).
[51]P. Gaspard, R. Kapral, and G. Nicolis, J. Stat. Phys. **35**, 697 (1984).
[52]P. Glendinning and C. Sparrow, J. Stat. Phys. **35**, 645 (1984).
[53]The normal form equations used in Ref. 34 have an additional fifth order term in $z$ with small coefficient.
[54]X. Wang and C. Y. Mou, J. Chem. Phys. **83**, 4554 (1985).
[55]F. Argoul and J. C. Roux, Phys. Lett. A **108**, 426 (1985).
[56]J. S. Turner, J. C. Roux, W. D. McCormick, and H. L. Swinney, Phys. Lett. A **85**, 9 (1981).
[57]J. C. Roux, J. S. Turner, W. D. McCormick, and H. L. Swinney, in *Nonlinear Problems: Present and Future*, edited by A. R. Bishop, D. K. Campbell, and B. Nicolaenko (North-Holland, Amsterdam, 1982), p. 409.
[58]D. Barkley, Phys. Lett. A **129**, 219 (1988).